Monthly Notices of the ROYAL ASTRONOMICAL SOCIETY

MNRAS **442,** 1586–1596 (2014) doi:10.1093/mnras/stu973

Near-infrared spectroscopy of young brown dwarfs in upper Scorpius

P. Dawson,[1⋆] A. Scholz,[2] T. P. Ray,[1] D. E. Peterson,[3] D. Rodgers-Lee[1] and V. Geers[1]

[1]*School of Cosmic Physics, Dublin Institute for Advanced Studies, 31 Fitzwilliam Place, Dublin 2, Ireland*
[2]*School of Physics & Astronomy, University of St Andrews, North Haugh, St Andrews, Fife KY16 9SS, UK*
[3]*Space Science Institute, 4750 Walnut Street, Suite 205, Boulder, CO 80301, USA*

Accepted 2014 May 13. Received 2014 March 26; in original form 2013 December 20

ABSTRACT

Spectroscopic follow-up is a pre-requisite for studies of the formation and early evolution of brown dwarfs. Here, we present Infrared Telescope Facility/SpeX near-infrared spectroscopy of 30 candidate members of the young Upper Scorpius association, selected from our previous survey work. All 24 high-confidence members are confirmed as young very low mass objects with spectral types from M5 to L1, 15–20 of them are likely brown dwarfs. This high yield confirms that brown dwarfs in Upper Scorpius can be identified from photometry and proper motions alone, with negligible contamination from field objects (<4 per cent). Out of the six candidates with lower confidence, five might still be young very low mass members of Upper Scorpius, according to our spectroscopy. We demonstrate that some very low mass class II objects exhibit radically different near-infrared (0.6–2.5 μm) spectra from class III objects, with strong excess emission increasing towards longer wavelengths and partially filled in features at wavelengths shorter than 1.25 μm. These characteristics can obscure the contribution of the photosphere within such spectra. Therefore, we caution that near-infrared derived spectral types for objects with discs may be unreliable. Furthermore, we show that the same characteristics can be seen to some extent in all class II and even a significant fraction of class III objects (∼40 per cent), indicating that some of them are still surrounded by traces of dust and gas. Based on our spectra, we select a sample of objects with spectral types of M5–L1, whose near-infrared emission represents the photosphere only. We recommend the use of these objects as spectroscopic templates for young brown dwarfs in the future.

Key words: techniques: photometric – open clusters and associations: individual: Upper Scorpius – infrared: stars.

1 INTRODUCTION

The discovery of brown dwarfs, objects with masses below the hydrogen-burning minimum mass, at solar abundances, of ∼0.075 $M_\odot$ (Chabrier & Baraffe 2000), has challenged our understanding of star formation. Numerous theories propose several methods for the formation of substellar objects by incorporating additional physical processes into models of star formation. These include: dynamic ejections, turbulent fragmentation, disc fragmentation or photoerosion of cores by hot stars (Whitworth et al. 2007). Constraining these scenarios provides a motivation for detailed studies of young brown dwarfs in diverse environments.

The first step for all observational studies of young brown dwarfs is deep survey work in nearby star-forming regions, with the goal of identifying and characterizing large samples. These samples can then be used to constrain the mass function, the disc properties, the binary fraction and other diagnostics for the star formation process. An excellent target for this purpose is the nearby Upper Scorpius (hereafter UpSco) star-forming region (Preibisch et al. 2002), which hosts a large population of brown dwarfs (Lodieu 2013), at a presumed age of 5–10 Myr (Preibisch et al. 2002; Pecaut, Mamajek & Bubar 2012). UpSco is at a distance of 145 ± 2 pc (de Zeeuw et al. 1999), while Preibisch et al. (2002) note that its members are spread in a roughly spherical volume of approximately 20 pc radius about this mean value. A recent examination of the composition of UpSco claims that it has solar metallicity (Mamajek et al. 2013). The region has little extinction (Ardila, Martin & Basri 2000), and measurable proper motion (Preibisch et al. 2002), which facilitates the identification of very low mass objects. It also has a disc fraction of only 23 per cent (Dawson et al. 2013). This means that the flux received comes mostly from photospheres with little contamination from discs. The young stars and brown dwarfs in UpSco are a dispersed population and cover 250 deg^2 on the sky; only the advent of deep wide-field surveys has made the study of the entire region possible.

⋆E-mail: dawsonp@tcd.ie

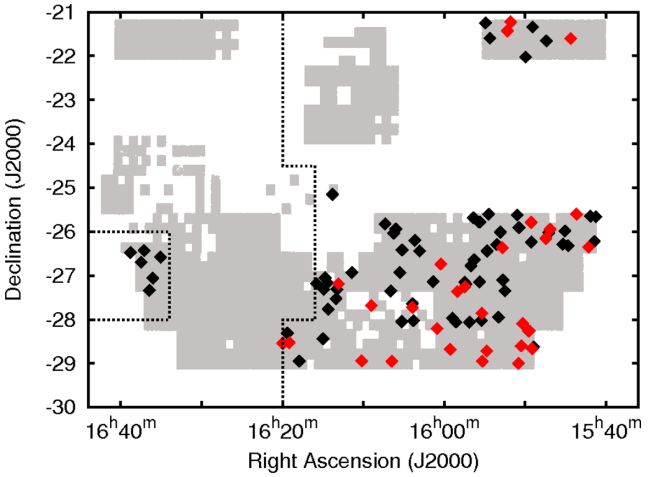

Figure 1. Coverage in *Z*, *Y*, *J*, *H* and *K* filters of 57 deg^2 in UpSco from the UKIDSS GCS. The diamonds mark the position of 96 candidate brown dwarfs as identified in Dawson et al. (2013) from the UKIDSS Ninth Data Release. The 30 objects investigated in this work are shown in red.

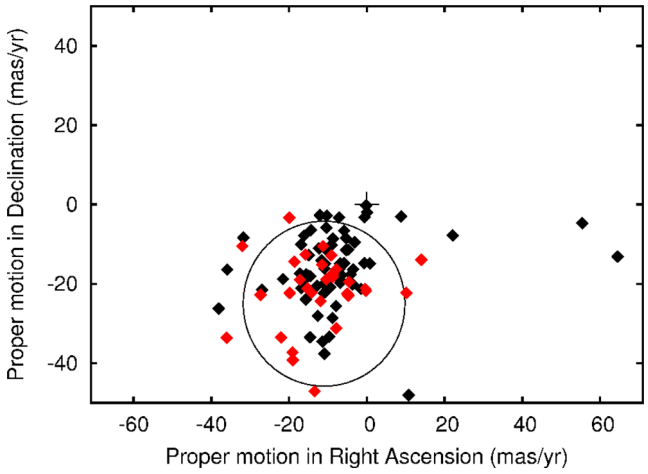

Figure 2. Vector-point diagram for 96 candidate brown dwarfs in UpSco as identified in Dawson et al. (2013) from the UKIDSS Ninth Data Release. There is an obvious and identifiable cluster around (−11,−25), while there is no significant clustering around the origin, indicating that there is very little contamination from background objects in the photometrically selected sample. The 20 candidates lying outside the 2σ selection circle were classified as non-members by Dawson et al. (2013). The 30 objects investigated in this work are shown in red.

In our previous papers, we have identified a list of brown dwarf candidates in UpSco based on the Galactic Cluster Survey that was carried out as part of the UKIRT Infrared Deep Sky Survey (UKIDSS; Dawson, Scholz & Ray 2011; Dawson et al. 2013). Our survey covered the southern part of the association and so it is complementary to previous work by other groups (Lodieu, Hambly & Jameson 2006; Slesnick, Carpenter & Hillenbrand 2006; Lodieu et al. 2007, 2008; Slesnick, Hillenbrand & Carpenter 2008; Lodieu, Dobbie & Hambly 2011; Lodieu 2013). Here, we present spectroscopic follow-up for a large number of these candidates. Our aims are twofold: to verify the nature of the sources and to examine the spectroscopic properties of the substellar objects in this region.

2 SAMPLE

A total of 30 objects from our survey (Dawson et al. 2011, 2013) were chosen for follow-up spectroscopy. They were chosen from a list of 96 candidate brown dwarfs identified from the UKIDSS Ninth Data Release. The magnitudes of the 30 are representative of those of the 96 from which they are taken. Their locations in UpSco are shown in Fig. 1. Dawson et al. (2013) showed that 24 of these objects have the photometric and proper motion characteristics of very low mass members of UpSco. As shown in the vector-point diagram in Fig. 2, they form part of a population of objects that lie inside a 2σ selection circle as calculated by Dawson et al. (2011) which is centred on the known proper motion of UpSco (−11, −25 mas yr^{-1}; de Bruijne et al. 1997; Preibisch et al. 2002) and hereinafter are referred to as 'the 2σ sample'. Of these 24 objects, 2 were first identified by Lodieu et al. (2006), 13 by Dawson et al. (2011) and the remaining 9 by Dawson et al. (2013). The other six objects were shown in Dawson et al. (2011, 2013) to have the photometric characteristics of very low mass members of UpSco. However, as shown in Fig. 2, they form part of a smaller population of objects that lie just outside the selection circle.

Based on mid-infrared photometry from the *WISE* satellite, Dawson et al. (2013) show that" 18 of the objects from the 2σ sample are class III objects (i.e. do not have a disc) while 6 of them are class II objects (i.e. have a disc). The six objects that lie outside the selection circle have been examined in the same manner as detailed in Dawson et al. (2013) for this work. They exhibit the 3.4–4.6 μm mid-infrared colours and weak 12 and 22 μm signals typical of class III objects in UpSco. None of the 30 objects had been spectroscopically investigated before. The 2MASS name and the position of each object are listed in Table 1. For the sake of simplicity and clarity, the objects are also numbered from 1 to 30 and are identified by these numbers throughout this work.

3 OBSERVATIONS

Spectra of the above targets were obtained during the nights of 2012 June 8–10 using the SpeX spectrograph (Rayner et al. 2003) at the NASA Infrared Telescope Facility (IRTF) on Mauna Kea. During the observing run, the IRTF was operated remotely from the offices of the Dublin Institute for Advanced Studies. Targets were observed with SpeX in single-prism mode covering a wavelength range of 0.8–2.5 μm. Slits used were either 0.″5 or 0.″8 × 15″, depending on the seeing. Airmass varied from 1.35 to 1.93 across the objects observed. Single exposure times used were either 60, 90 or 120 s. Spectra were also obtained of several A0 V stars in the vicinity of the 30 targets. These spectra of standard stars were used to correct for telluric absorption in the target spectra. As detailed in Cushing, Vacca & Rayner (2004), SpeX has an external calibration unit containing the lamps needed for flat-fielding and wavelength calibration. Exposures of these lamps were taken three times during each observing night. Table 1 details the slit width used, the airmass, single exposure time and associated standard star for all 30 objects.

4 DATA REDUCTION

The raw spectra were reduced" with SPEXTOOL, an IDL-based spectral reduction package designed specifically for use with data obtained from SpeX (Cushing et al. 2004). Flat-field and wavelength calibration exposure frames were made using the SPEXTOOL package. The target object spectra and the standard star spectra were then

Table 1. Summary of SpeX observations. The first 24 objects are those in the 2σ sample (see the text, Section 2). The last six objects have proper motions that caused Dawson et al. (2013) to classify them as non-members of UpSco (also see the text, Section 2). The names and positions of the objects are listed, followed by details from the observation records for each; slit width used, airmass, single exposure time and associated standard star.

Object number	2MASS name	RA J2000	Dec. J2000	Slit width (arcsec)	Airmass	Single exposure time (s)	Standard star
1	2MASSJ15420830-2621138	15:42:08.31	−26:21:13.8	0.5	1.73	60	HD 143747
2	2MASSJ15433947-2535549	15:43:39.47	−25:35:54.9	0.5	1.53	120	HD 143747
3	2MASSJ15442275-2136092	15:44:22.75	−21:36:09.3	0.5	1.50	90	HD 143747
4	2MASSJ15465432-2556520	15:46:54.32	−25:56:52.1	0.5	1.56	60	HD 143747
5	2MASSJ15472572-2609185	15:47:25.73	−26:09:18.5	0.5	1.82	60	HD 138813
6	2MASSJ15490803-2839550	15:49:08.02	−28:39:55.2	0.8	1.55	90	HD 143822
7	2MASSJ15491602-2547146	15:49:16.02	−25:47:14.6	0.5	1.67	60	HD 138813
8	2MASSJ15492909-2815384	15:49:29.08	−28:15:38.6	0.8	1.93	90	HD 138813
9	2MASSJ15493660-2815141	15:49:36.59	−28:15:14.3	0.5	1.92	90	HD 138813
10	2MASSJ15501958-2805237	15:50:19.58	−28:05:23.9	0.8	1.63	120	HD 143822
11	2MASSJ15514709-2113234	15:51:47.09	−21:13:23.5	0.5	1.37	60	HD 136602
12	2MASSJ15521088-2125372	15:52:10.88	−21:25:37.4	0.5	1.35	60	HD 136602
13	2MASSJ15524857-2621453	15:52:48.57	−26:21:45.4	0.5	1.49	60	HD 143747
14	2MASSJ15544486-2843078	15:54:44.85	−28:43:07.9	0.5	1.63	90	HD 138813
15	2MASSJ15551960-2751207	15:55:19.59	−27:51:21.0	0.5	1.56	90	HD 143822
16	2MASSJ15572692-2715094	15:57:26.93	−27:15:09.5	0.5	1.48	60	HD 143747
17	2MASSJ15582376-2721435	15:58:23.76	−27:21:43.7	0.5	1.50	90	HD 146606
18	2MASSJ15591513-2840411	15:59:15.12	−28:40:41.3	0.8	1.87	90	HD 143882
19	2MASSJ16002535-2644060	16:00:25.35	−26:44:06.1	0.5	1.58	60	HD 143747
20	2MASSJ16005265-2812087	16:00:52.66	−28:12:09.0	0.5	1.84	90	HD 138813
21	2MASSJ16062870-2856580	16:06:28.70	−28:56:58.2	0.5	1.68	90	HD 143747
22	2MASSJ16090168-2740521	16:09:01.68	−27:40:52.3	0.8	1.74	90	HD 143822
23	2MASSJ16101316-2856308	16:10:13.15	−28:56:31.0	0.8	1.56	90	HD 143747
24	2MASSJ16195827-2832276	16:19:58.26	−28:32:27.8	0.5	1.57	120	HD 143822
25	2MASSJ15502934-2835535	15:50:29.32	−28:35:53.9	0.8	1.53	120	HD 143747
26	2MASSJ15504920-2900030	15:50:49.19	−29:00:03.1	0.8	1.53	90	HD 146606
27	2MASSJ15551768-2856579	15:55:17.70	−28:56:58.1	0.5	1.52	60	HD 143822
28	2MASSJ16035601-2743335	16:03:56.00	−27:43:33.6	0.8	1.48	90	HD 143747
29	2MASSJ16130482-2711214	16:13:04.84	−27:11:21.8	0.5	1.50	90	HD 146606
30	2MASSJ16190983-2831390	16:19:09.82	−28:31:39.5	0.5	1.53	90	HD 143822

extracted. Telluric absorption features in the target object spectra were subsequently removed using the standard star spectra and the *xtellcor* IDL widget within the SPEXTOOL package, using the method of Vacca, Cushing & Rayner (2003). The spectra were then normalized at the 1.25 μm *J* band to facilitate comparison with each other. The spectra are shown in Figs 3 and 5–8.

5 SPECTRAL ANALYSIS

The primary aim of the spectral analysis was to determine the spectral type of each object in order to confirm its nature as a young very low mass object in UpSco. For solar abundance brown dwarfs with $0.013 < M < 0.075\,M_{\odot}$ (Chabrier & Baraffe 2000), we expect the spectral type to range from about M6 to L0 at the age of this region (5–10 Myr). For this range of spectral types, we expect the near-infrared spectra to show a peak in the *H* band at 1.68 μm and another in the *K* band at 2.25 μm. These peaks are caused by H_2O absorption features at 1.3–1.5 μm and another at 1.75–2.05 μm and can be used as a diagnostic for objects of M-type and later. The shape of the *H*-band peak is gravity sensitive, being sharply defined in young objects and much less well defined in evolved objects, exhibiting a plateau in the region on the blue side of 1.68 μm (Kirkpatrick, Barman & Burgasser 2006; Peterson et al. 2008). In addition, late-type objects exhibit a steep edge at 1.35 μm, again caused by H_2O absorption and CO absorption bands at 2.3 μm. For a more detailed discussion of infrared spectra of M–L type objects, see Cushing, Rayner & Vacca (2005) and Scholz et al. (2009).

5.1 Spectral sequence

Inspection of the spectra showed that each object in our sample exhibited a peak in the *H* band at 1.68 μm. Its presence in each spectrum indicates that all the objects examined are M- or L-type objects. Later objects within this range are expected to have deeper troughs, and hence steeper slopes, on both the *J* and *K* side of the peak in the *H* band. The consequent prominence of the *H*-band peak becomes correspondingly less in earlier type objects that have shallower troughs and slopes on either side of the peak. The spectra were plotted and then arranged by eye in a sequence, from earliest to latest, based on a comparison of the shape of each spectrum in the vicinity of the peak in the *H* band (first, second and third panels in Fig. 3).

It is clear from Fig. 3 that object 30 in the third panel has a more rounded *H*-band peak than the others, indicating that it is an old field object rather than a young substellar member of UpSco. It is one of the six objects shown in Fig. 2 which lie outside the selection circle.

We compared the sequence of spectra in the first, second and third panels of Fig. 3, with templates of young late-type objects that had been given spectral types based on their optical spectrum. This comparison was carried out to further calibrate our visually

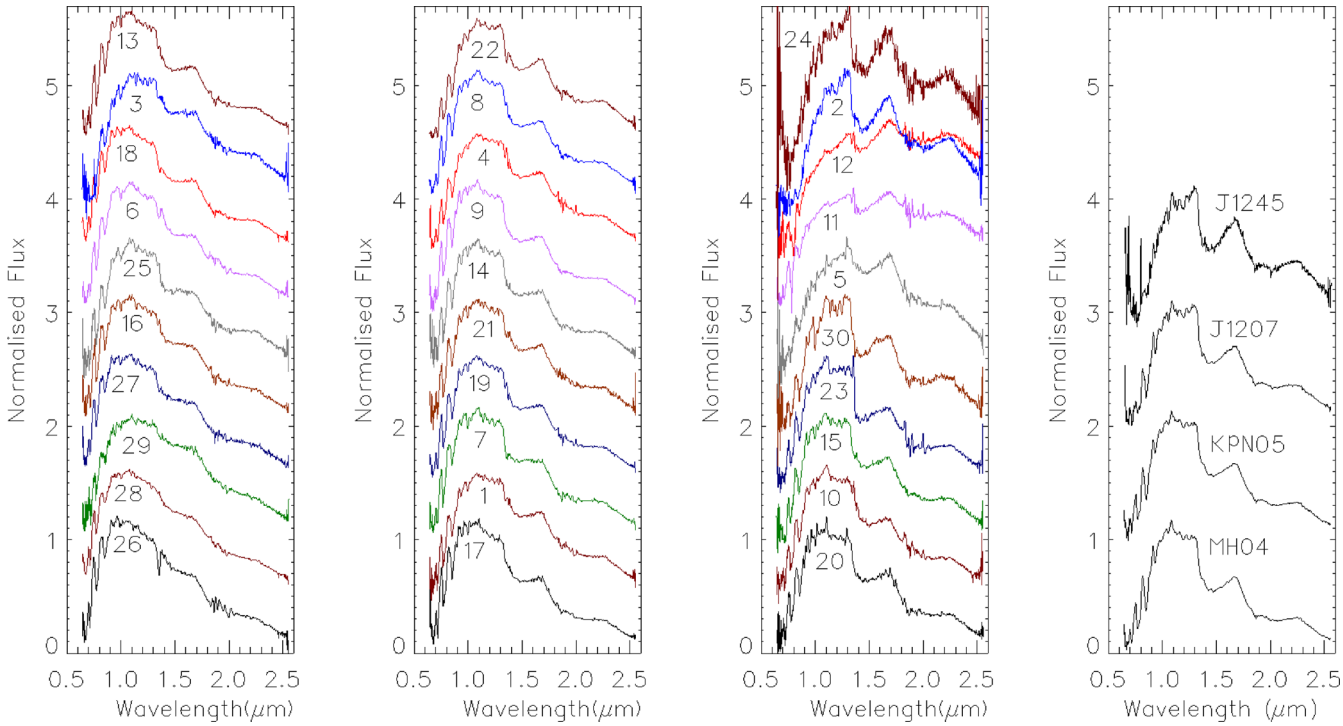

Figure 3. Spectra of all 30 targets arranged in order of the prominence of the peak in the *H* band at 1.68 μm. Also shown in the fourth panel are the spectra of four templates with known spectral types for comparison (from bottom to top: M7, M7.5, M8 and M9.5). Spectra are normalized at 1.25 μm (*J*) and offset by 0.5. The different profiles of the spectra of the class II objects (5, 11 and 12) in the third panel are quite distinct (see the text, Section 6.1).

arranged spectral sequence. The templates were taken from the SpeX library on www.browndwarfs.org.[1] The selected templates are: MHO4 (M7), KPNO5 (M7.5), J1207 (M8) and J1245 (M9.5), taken from Muench et al. (2007) and Looper et al. (2007) and are shown in the fourth panel in Fig. 3. Judged by their near-infrared colours, these four show little extinction ($A_V < 1$ mag, see Scholz et al. 2012) and so are comparable with the UpSco sample. The conclusion from this visual comparison of the templates and sample objects was that about a third of the objects were within half a subtype of M7 (second panel in Fig. 3), while about a third were earlier (first panel) and the remaining third were later than M7.5 (third panel).

The ordering of the spectra and their visual comparison with the template objects had established that most of the objects appear to be young and of late M type, apart from object 30 which was determined to be an evolved field object with a type of M8.

5.2 Spectral indices

In order to derive spectral types, we use and compare three spectral definitions that have been used in the recent literature. The analysis of each spectrum and calculation of each index was performed using IDL routines.

5.2.1 The H-peak index

Described in Scholz et al. (2012), the *H*-peak index (HPI) is defined as the ratio of the fluxes measured in the intervals between 1.675–1.685 μm and 1.495–1.505 μm. The first interval in this ratio is at the position of the peak in the *H* band (Fig. 3). The second interval is located near the flux minimum on the blue side of the peak. The HPI therefore utilizes the maximum flux range available between the bottom of the H_2O absorption band at 1.3–1.5 μm and the peak in flux at 1.68 μm. Scholz et al. (2012) determined an empirical relationship between the HPI and spectral types for the range from M7 to M9.5, noting that this relationship may also hold for spectral types later than M9.5, but does not apply for spectral types earlier than M7. The correlation between the HPI and spectral type (SpT) is given by Scholz et al. (2012) as

$$\mathrm{SpT} = -0.84 + 7.66 \times \mathrm{HPI}. \quad (1)$$

In our sample, 20 of the objects are classified as M7 or later via the HPI, with L0.3 as the latest type (Table 2 and Fig. 4). The remaining 10 are all given spectral types of between M6.1 and M6.9. Notably, five of the six objects from outside the selection circle in Fig. 2 are among those with spectral types earlier than M7. The sixth object from outside the selection circle is object 30 with a spectral type of M8.4, but – as noted above – this is the object with the plateau near the *H*-band peak suggesting that it is a field object too old to be a member of UpSco.

In summary, of the 24 objects from the 2σ sample, the HPI categorizes 18 of them as young very low mass objects, with spectral types of M7.0–L0.3, placing them all within the brown dwarf mass regime.

5.2.2 The H_2O index

The H_2O index devised by Allers, Jaffe & Luhman (2007) uses the ratio of the fluxes in the intervals between 1.550–1.560 μm and 1.492–1.502 μm to characterize spectra. Compared to the HPI it utilizes a shorter part of the same slope on the blue side of the

[1] See http://pono.ucsd.edu/~adam/browndwarfs/spexprism/.

Table 2. UKIDSS *Z* photometry, Class, HPI and spectral type, H_2O index and spectral type, H_2O–K2 index and spectral type of the 30 objects observed with SpeX. Objects are listed in the same order as in Table 1.

Object number	2MASS name	*Z* mag	Object class	*H*-peak index	*H*-peak spectral type	H_2O index	H_2O spectral type	H_2O–K2 index	H_2O–K2 spectral type
1	2MASSJ15420830-2621138	15.15	III	1.05	M7.2	1.01	M5.8	0.80	M5.7
2	2MASSJ15433947-2535549	18.15	II	1.36	M9.5	1.16	M9.4	0.61	L0.1
3	2MASSJ15442275-2136092	16.55	III	0.92	M6.2	1.01	M5.9	0.77	M6.3
4	2MASSJ15465432-2556520	14.16	II	1.06	M7.3	1.01	M5.9	0.80	M5.7
5	2MASSJ15472572-2609185	15.40	II	1.14	M7.9	1.04	M6.6	0.79	M5.9
6	2MASSJ15490803-2839550	14.82	III	0.97	M6.6	0.99	M5.5	0.81	M5.3
7	2MASSJ15491602-2547146	14.31	III	0.99	M6.7	1.01	M5.9	0.79	M5.9
8	2MASSJ15492909-2815384	14.29	III	1.07	M7.3	1.03	M6.4	0.77	M6.5
9	2MASSJ15493660-2815141	14.66	III	1.06	M7.3	1.03	M6.3	0.79	M6.0
10	2MASSJ15501958-2805237	16.04	II	1.07	M7.4	1.03	M6.4	0.76	M6.7
11	2MASSJ15514709-2113234	15.12	II	1.13	M7.8	1.04	M6.6	0.90	M3.3
12	2MASSJ15521088-2125372	15.72	II	1.21	M8.5	1.07	M7.2	0.88	M3.7
13	2MASSJ15524857-2621453	14.62	III	1.04	M7.1	1.02	M6.1	0.79	M6.0
14	2MASSJ15544486-2843078	15.51	III	1.04	M7.1	1.01	M5.9	0.78	M6.1
15	2MASSJ15551960-2751207	15.60	III	1.13	M7.8	1.04	M6.6	0.73	M7.4
16	2MASSJ15572692-2715094	14.93	III	0.94	M6.4	1.00	M5.5	0.84	M4.7
17	2MASSJ15582376-2721435	14.35	III	1.00	M6.9	1.00	M5.7	0.80	M5.6
18	2MASSJ15591513-2840411	14.14	III	1.00	M6.8	0.99	M5.5	0.80	M5.7
19	2MASSJ16002535-2644060	14.38	III	1.05	M7.2	1.01	M5.9	0.78	M6.2
20	2MASSJ16005265-2812087	15.04	III	1.05	M7.2	1.02	M6.1	0.75	M6.8
21	2MASSJ16062870-2856580	14.90	III	1.09	M7.5	1.02	M6.2	0.82	M5.2
22	2MASSJ16090168-2740521	14.33	III	1.13	M7.8	1.03	M6.2	0.75	M6.9
23	2MASSJ16101316-2856308	15.67	III	1.12	M7.8	1.09	M7.7	0.70	M8.0
24	2MASSJ16195827-2832276	18.74	III	1.45	L0.3	1.24	L1.1	0.59	L0.8
25	2MASSJ15502934-2835535	16.05	III	0.99	M6.7	1.03	M6.4	0.75	M6.9
26	2MASSJ15504920-2900030	14.35	III	0.91	M6.2	0.98	M5.2	0.90	M3.4
27	2MASSJ15551768-2856579	14.32	III	0.96	M6.5	0.99	M5.4	0.93	M2.6
28	2MASSJ16035601-2743335	14.41	III	0.91	M6.1	0.98	M5.3	0.88	M3.7
29	2MASSJ16130482-2711214	15.56	III	0.92	M6.2	0.99	M5.4	0.89	M3.5
30	2MASSJ16190983-2831390	16.63	III	1.20	M8.4	1.13	M8.7	0.72	M7.5

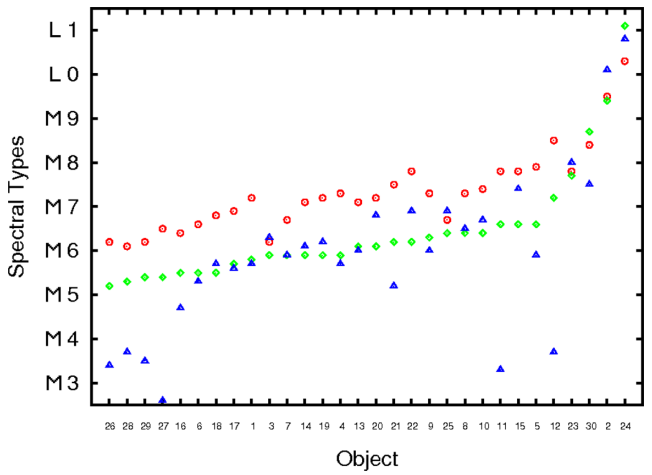

Figure 4. Spectral types of all 30 objects as derived via the *H*-peak (red circles), H_2O (green diamonds) and H_2O–K2 (blue triangles) indices. Objects are ordered in terms of their H_2O index spectral type. The H_2O and *H*-peak indices give similar spectral types for each object, the H_2O index results tending to be 1 subtype earlier. 24 of the H_2O–K2 index spectral types agree to within 1 subtype with at least one of the other indices, while the remaining six have anomalously earlier types (see the text, Section 5.2).

H-band peak. The correlation between the H_2O index and spectral type given by Allers et al. (2007) is

$$H_2O = 0.75 + 0.044 \times \mathrm{SpT}. \quad (2)$$

Allers et al. (2007) state that the relationship is independent of gravity and can be used to determine spectral types for field dwarfs, giants and young brown dwarfs over the spectral type range of M5–L0.

Using the H_2O index, all 30 objects in our sample are classified as M5 or later with 16 of the objects classified as M6 or later, and with L1.1 as the latest spectral type (Table 2). These spectral types tend to be 1 subtype earlier than those given by the HPI (see Fig. 4), as already noted by MuzŽić et al. (2012). Four of the Five objects from outside the selection circle in Fig. 2, which are classified among the earliest spectral types via the HPI, are also assigned the earliest spectral types (M5.2–M5.4) via the H_2O index. The other (object 25) is classified as an M6.4 object, while the field dwarf (object 30) is given a spectral type of M8.7.

The 24 objects from the 2σ sample are all given spectral types of M5.5 and later. Therefore, the H_2O index classifies all of these 24 objects as very low mass members of UpSco ranging from the lowest stellar masses to the lower end of the mass range of brown dwarfs.

5.2.3 *The H_2O–K2 index*

The H_2O–K2 index was devised by Rojas-Ayala et al. (2012) to represent the change in the overall shape of the spectra of M dwarfs due to water absorption in the *K* band from 2.07 to 2.38 μm. It uses the ratio of two ratios, i.e. the ratio of the fluxes between 2.070–2.090 μm and 2.235–2.255 μm to the ratio of the fluxes between

2.235–2.255 μm and 2.360–2.380 μm. For objects between spectral types M0 and M9 Rojas-Ayala et al. (2012) gives the relationship between spectral type and H_2O–K2 index as

$$\mathrm{SpT} = 24.699 - 23.788 \times H_2O{-}K2. \quad (3)$$

As can be seen in Table 2 and Fig. 4, the H_2O–K2 index spectral types agree with the H_2O index to within 1 subtype for most (23/30) of the objects. However, the H_2O–K2 index returns 2 markedly earlier spectral types, M3.3 and M3.7, for objects 11 and 12, respectively. They have HPI spectral types of M7.8 and M8.5 and H_2O index spectral types of M6.6 and M7.2. These are two of the class II objects which can be seen in Fig. 3 to have distinctly different spectral profiles to most of the other objects. They were shown in Dawson et al. (2013) to exhibit an obvious excess in their near-infrared J–K colours, the result of excess emission in the *K* band from circumsubstellar discs. So the H_2O–K2 index is measuring that part of their near-infrared spectral profiles which Dawson et al. (2013) have already shown is mostly non-photospheric in origin. Apart from these two objects all the objects from the 2σ sample are classified with spectral types ranging from M4.7 to L0.8.

Of the objects that are not in the 2σ sample, objects 26, 27, 28 and 29 are given spectral types varying from M2.6 to M3.7, about 2 or more subclasses earlier than their H_2O index spectral types. The field dwarf, object 30, is given a spectral type of M7.5, earlier than its H_2O index classification of M8.7, while object 25 is assigned spectral type M6.9, similar to its H_2O index derived type of M6.4.

With the exception of objects 11 and 12, the H_2O–K2 index yields spectral types of M4.7 and later for the objects in the 2σ sample, which again classifies them as very low mass members of UpSco ranging from the lowest stellar masses down into the mass range of brown dwarfs.

5.3 Summary of spectral classifications

We determined spectral types from comparisons with templates and with three different spectral indices in the *H* and *K* bands. The types are listed in Table 2 and shown in Fig. 4. The overall results are summarized as follows.

(1) The 24 objects from the 2σ sample have spectral types ranging from M5 to L1, with about 20 being of type M6 or later and they all exhibit evidence for youth. This classifies them as likely brown dwarfs and young members of UpSco.

(2) Of the six other objects, one of them is a field M8–M9 dwarf (and is most probably in the foreground) while the remaining five are early- to mid-type (M3–M6) young M dwarfs. These 5 could still be members of UpSco, but with slightly different kinematical characteristics.

5.4 Contamination

Dawson et al. (2013) demonstrated that there was minimal contamination of the sample of 76 brown dwarf members of UpSco identified from the UKIDSS Ninth Data Release, based on the distribution of the proper motion vectors.

The spectral types of the 24 objects in the 2σ sample obtained via the methods outlined above confirm that each one is a young object with a spectral type between M5 and L1, classifying them as either brown dwarfs or very low mass stars. Ergo, there is no measurable contamination in this sample ($<1/24$, i.e. <4 per cent). This confirms the efficacy of using photometric and proper motion data from both the UKIDSS Galactic Cluster Survey and 2MASS as outlined in Lodieu et al. (2006, 2007), Lodieu (2013) and Dawson et al. (2011, 2013) to reliably identify brown dwarf members of UpSco.

6 DISCUSSION OF SPECTRAL TYPES

Each object in our sample had spectral types assigned to it using different indices that measured specific parts of each spectrum. Spectra of objects with similar types were compared to each other to see how closely their overall profiles matched.

6.1 Divergence of class II and class III spectra

The spectra shown in Fig. 3 include three that display radically different profiles from all the others. These objects (5, 11 and 12) were shown in Dawson et al. (2013) to be class II objects, based on their *WISE* photometry in the *W*1 (3.4 μm) and *W*2 (4.6 μm) bands. Objects 11 and 12 were also the only 2 of 27 class II objects analysed in Dawson et al. (2013) to exhibit an obvious excess in their near-infrared $J - K$ colours. The differences in profile can be seen more clearly in Fig. 5, which compares these spectra with the spectra of three of the class III objects (15, 22 and 23). All six objects have similar HPI spectral types, the class III objects all being of type M7.8, while objects 5, 11 and 12 are of type M7.9, M7.8 and M8.5, respectively. The class III objects have very similar spectra. The class II objects, on the other hand, have quite different spectra from the class III objects, and each other. However, there are several features common to the class II spectra: (1) the most obvious feature is the higher normalized flux levels at the *H*- and *K*-band peaks relative to the *J* band, (2) the profiles of the class II spectra in the region on the blue side of the *J* band share a distinctive rounded shape, generally being deficient in normalized flux in this wavelength range by comparison with the class III objects, (3) features in this part of the class II spectra also tend to be attenuated. In particular, the TiO feature at 0.84 μm tends to be much weaker among the class II objects. Taken together, the presence of these characteristics in a spectrum appear to be diagnostic of a class II object. An examination of the other class II objects in the sample (2, 4 and 10) showed that they exhibit these same characteristics when compared to class III objects of similar spectral type.

The most likely origin of these spectral features is excess emission from a circumsubstellar disc. In these objects, warm dust from the inner disc absorbs photospheric light and emits it at longer wavelengths. This causes the observed excess in the near-infrared bands. As seen in Fig. 5, the excess becomes stronger from the *J* to the *K* band. At the blue end of our spectra, the attenuation of the photospheric features is similar to the veiling observed in T-Tauri stars, a phenomenon which has been attributed, at least in part, to accretion processes (Hartigan et al. 1991; Folha & Emerson 1999).

The presence of these characteristics raises questions about the reliability of the spectral typing of class II objects using near-infrared spectra. If the flux at wavelengths longer than *J* contains significant contributions from a dusty disc, the shape of the *H*-band or *K*-band peak cannot be relied upon to represent the shape of the underlying photospheric spectrum. Fig. 5 shows that contributions from the discs of the class II objects seem to be altering the shape of the spectra in the region of the *K* band by filling in the H_2O absorption band at 1.75–2.05 μm. This appears to be the reason that the H_2O–K2 index yielded much earlier spectral types for objects 11 and 12 than the other indices. Moreover, it is also clear from Fig. 5 that the spectra of the class II objects also have significant contributions from their discs in the region of the *H* band. Without a clear

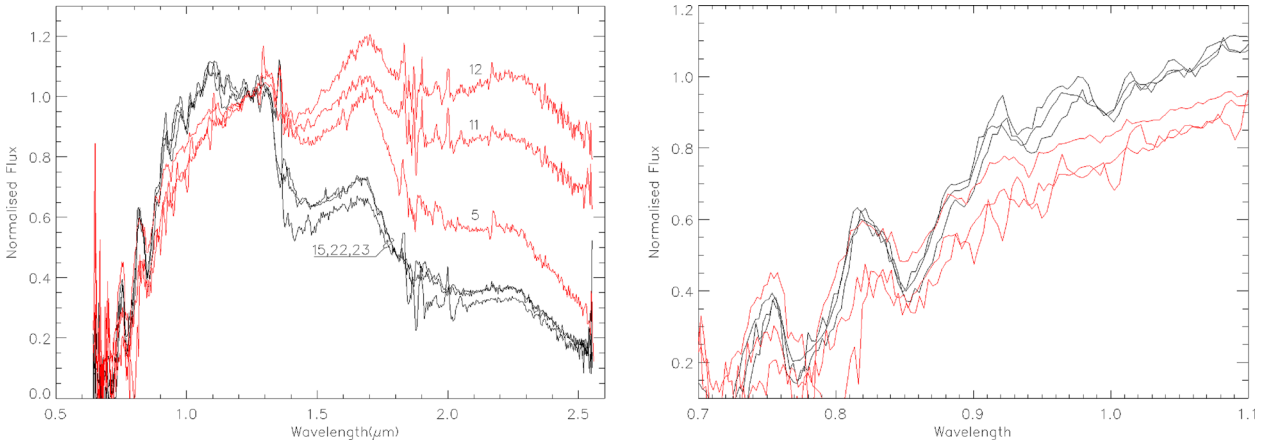

Figure 5. Spectra for three class III objects classified as spectral type M7.8 via the HPI are shown in black. Overplotted in red are the spectra of three class II objects with HPI spectral types (reading from bottom to top) of M7.9, M7.8 and M8.5. All spectra are normalized at 1.25 μm and are not offset. The radically different shapes of the class II spectra are readily apparent in the left-hand panel. The right-hand panel shows the shorter wavelength part of the spectra in more detail. In this region, the class II spectra are mostly deficient in normalized flux and their features are weak by comparison with the class III spectra (see the text, Section 6.1).

understanding of how that part of the spectral profile is affected by contributions from the disc it is impossible to be confident that the spectral types derived from the *H*-peak and H_2O indices are any more reliable than the H_2O–K2 index spectral types for these three objects.

Fig. 5 indicates that to obtain a reliable spectral type of a class II brown dwarf using near-infrared spectroscopy, the overall shape of the spectrum from 0.8 to 2.5 μm needs to be taken into account. If it resembles that of the class II objects in Fig. 5, any spectral type derived using only a small part of this wavelength range should be regarded as provisional. For such objects, the most reliable spectral types might still only be obtained from optical data. Thus, we caution against relying on near-infrared spectra for spectral typing of objects with known excess emission from a disc.

6.2 Diversity of class III spectra

The class III spectra show a lesser, but still significant diversity between objects of the same spectral type. In the following, we illustrate this by comparing spectra of class III objects with similar spectral types.

Fig. 6 shows the spectra of class III objects 1, 9, 13 and 19, all of which are classified between M7.1 and M7.3 using the HPI. The spectra have similar shapes on the blue side of the *H*-band peak. However, in the *H* and *K* band, object 1 has higher normalized flux levels (by ∼10 per cent) than the other objects and its features are a little shallower at the shorter wavelengths. The characteristics seen in the spectrum of object 1 are qualitatively similar to the appearance of the class II spectra (Section 6.1).

The same pattern of diversity can be seen between the spectra of the class III objects 7, 14 and 19 and the class II object 4 in Fig. 7. All have spectral types of M5.9 as determined via the H_2O index. Object 4 exhibits slight traces of the class II characteristics seen in Fig. 5. It has higher normalized flux levels in the *H* band, while at the shorter wavelengths it exhibits a deficiency in normalized flux and attenuated features.

The spectrum of object 1 is very similar to that of object 4 in Fig. 8, where they are shown along with the class III objects 17 and 18. All are classified as type M5.6 or M5.7 via the H_2O–K2 index. The similarity of objects 1 and 4 is such that it appears that the spectrum of object 1 is not completely photospheric in origin but also contains small contributions from a dusty disc. This tallies with its position in Fig. 6. Objects 17 and 18 have lower normalized flux levels on the red side of *J* and display higher levels on the blue side of *J*, indicating that their spectra are more photospheric in origin.

In summary, the differences between the spectra shown in Figs 6–8 are of a similar pattern to the differences between the class II and class III objects shown in Fig. 5, albeit at a lower level. Compared with the cases shown in Fig. 5, the observed spectral diversity is small and does not affect the spectral type significantly (i.e. by more than 1 subtype).

The class II like characteristics are present in 7 of the 18 (∼40 per cent) class III objects in the 2σ sample.

The nature of the anomalous emission observed in some class III objects remains unclear. It is conceivable that the spectral diversity in the class III objects is related to the presence of traces of dust and gas surrounding these objects. One possibility is that these objects represent an intermediate stage – a class II.5 as it were – between the objects with bona fide discs and the 'clean and clear' class III sources without any evidence for excess emission.

Alternately, the diversity among the class III spectra may be due to reddening. To test this, we artificially reddened the spectra of objects 13, 17, 18, 19 and 23, and compared them with those of the other objects. To redden the spectra, we used the near-infrared extinction law

$$\left(\frac{A_\lambda}{A_J}\right) = \left(\frac{\lambda}{1.25\,\mu\mathrm{m}}\right)^{-\alpha} \quad (4)$$

with a value of 1.7 for α, as given by Mathis (1990), and took $A_J = 0.282A_V$ (Rieke & Lebofsky 1985). We then adapted the method used by Rayner, Cushing & Vacca (2009), to correct for reddening in spectra obtained with SpeX, and reddened each spectrum using a range of values for A_V between 1 and 10. In each case, the least reddened spectra differed from the original spectrum in a manner that closely resembled the pattern of differences shown in Figs 6–8.

The differences that were observed are typified by the example shown in Fig. 9. Reddened spectra of object 19 are plotted alongside its real spectrum and compared to the spectrum of object 1. Both objects (which also feature in Figs 6–8) are classified as M7.2 using the HPI. The spectrum of object 1 most closely resembles the

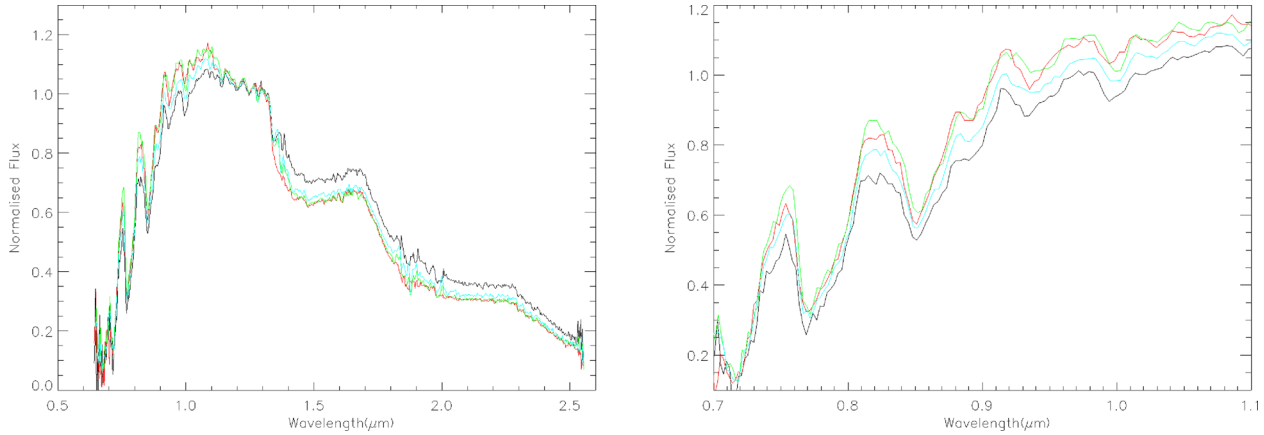

Figure 6. Spectra for objects 1 (black), 9 (red), 13 (green) and 19 (blue), all classified via the HPI as having spectral types between M7.1 and M7.3. In the left-hand panel, the similar profiles of the spectra in the region blue of the *H*-band peak are obvious. However, object 1 displays noticeably higher normalized flux levels in this region, and in the region blue of *J* most of its features are shallower than those of the other objects. The right-hand panel shows the latter region in more detail. Object 1 has the shallowest TiO feature at 0.84 μm.

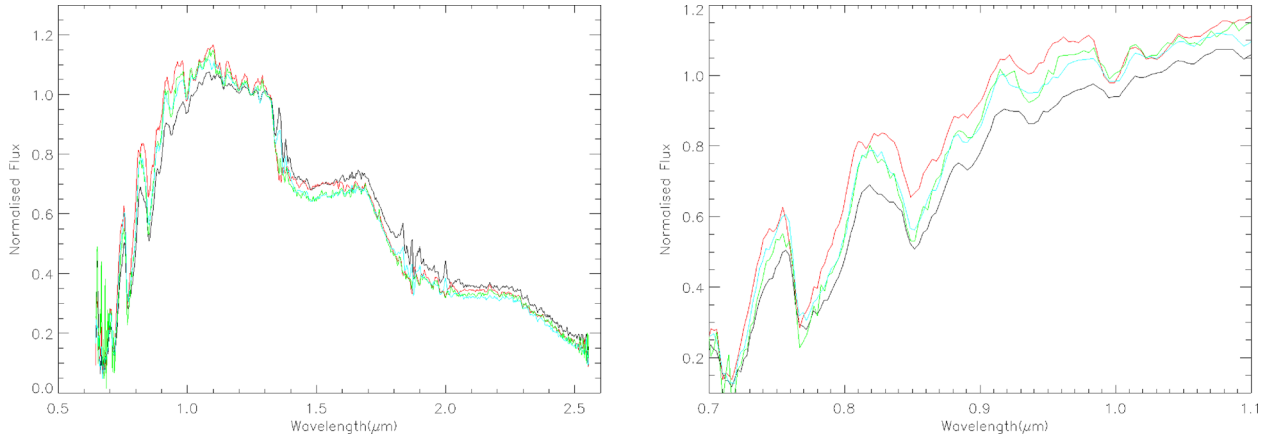

Figure 7. Spectra for objects 4 (black), 7 (red), 14 (green) and 19 (blue), all classified as spectral type M5.9 via the H_2O index. Object 4 is a class II object and it has the highest normalized flux levels in the region red of *J* (left-hand panel) along with the lowest levels in the region blue of *J* (shown in detail in the right-hand panel), where its features are also visibly weaker by comparison with objects 14 and 19. These are the same traits exhibited by the class II objects shown in Fig. 5, albeit on a lesser scale.

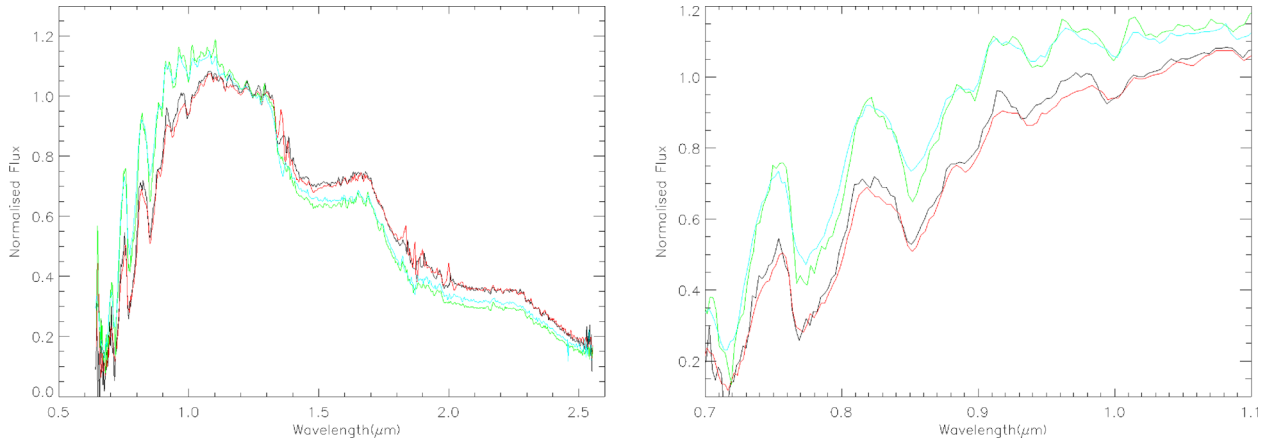

Figure 8. Spectra for objects 1 (black), 4 (red), 17 (green) and 18 (blue) classified as spectral types M5.6 and M5.7 via the H_2O–K2 index. In these graphs, the spectra of the class III objects 17 and 18 can be seen to be very similar to each other, and distinct from those of objects 1 and 4. The spectrum of the class III object 1 has a shape very similar to that of the class II object 4 (see the text, Section 6.2).

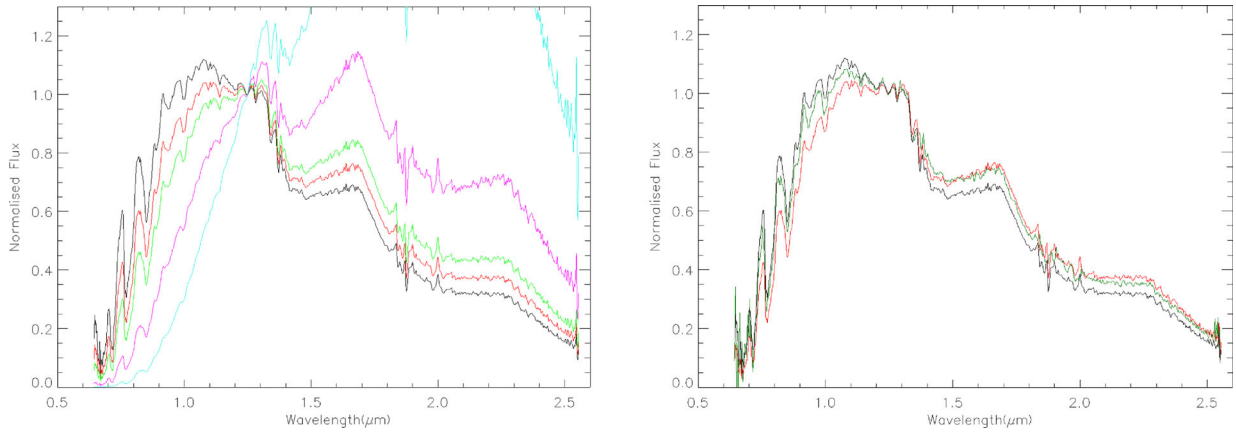

Figure 9. Spectrum of object 19, with artificially reddened spectra overplotted (left-hand panel). The original spectrum (black) is the one with the lowest normalized flux in the vicinity of the *H*-band peak. The four reddened spectra represent A_V of 1 (red), 2 (green), 5 (pink) and 10 (blue). The right-hand panel shows the spectrum of object 1 (dark green), overlaid on the unreddened, and slightly reddened ($A_V = 1$) spectra of object 19 (black and red, respectively). The spectrum of object 1 is similar to the least reddened spectrum of object 19 (see the text, Section 6.2).

spectrum of object 19 that has been reddened using an $A_V = 1$. An $A_V = 1$ is within the limits of the little extinction that exists in the region of UpSco where the objects are located (Ardila et al. 2000). On this basis, a plausible amount of interstellar reddening could account for the diversity among the spectra of the class III objects.

Reddening alone is not a plausible cause of the different shape of the spectra of the class II objects shown in Fig. 5. Objects 5 and 11 have similar spectral types (M7.8 and M7.9 via the HPI), and yet their spectra are very different *to each other*, as well as to the spectra of the class III objects in the same diagram. No single reddening law could produce a match for both spectra. A comparison with the reddened spectra of object 23 (which has a similar HPI spectral type of M7.8), also shows that none of its reddened spectra are a match for the spectra of objects 5 or 11. Therefore, while reddening may be present in these cases, it cannot be the predominant cause of the diversity among these class II spectra. Nor, if present, can it be readily distinguished from the overwhelming contributions of the circumsubstellar discs.

All the class II objects in this survey were shown in Dawson et al. (2013) to have excess flux in the mid-infrared. The objects with the largest mid-infrared excess were also shown to have a corresponding contiguous excess in the near-infrared, as shown in figs 4 and B1 of Dawson et al. (2013). All of the class II objects exhibit these characteristics, although they may be present to a much lesser extent, while they are present in only ∼40 per cent of the class III objects, in the 2σ sample. Among the class III spectra that exhibit these characteristics, disentangling the relative contributions of small amounts of excess emission, veiling and reddening involved is not possible. Therefore, although near-infrared spectroscopy may be more sensitive to residual disc emission than mid-infrared photometry, it does not, in these cases, provide the robust certainty required for identifying circumsubstellar discs that is provided by mid-infrared photometry. In each case, whatever the exact cause of these effects, the underlying photospheric spectrum is being obscured and distorted.

6.3 Templates for spectral typing

There is a need for a catalogue of spectral templates of young brown dwarfs that are clean and clear of the effects of veiling, excess emission and reddening, in order to establish benchmarks that can be used to correct for these effects. The spectra of the 24 objects in the 2σ sample were examined with the intent of producing a sequence of template spectra of young brown dwarfs that are free of contributions from any source other than their photospheres. Our spectroscopic survey is ideal for producing such a catalogue for two reasons: (1) UpSco is not significantly affected by extinction, (2) the disc fraction in UpSco (23 per cent) is low by comparison with other young star-forming regions (Dawson et al. 2013), which maximizes the chances of obtaining spectra that are purely photospheric in origin.

In a first step, objects 5, 11 and 12 – the class II objects from Fig. 5 – were summarily disregarded. Object 4 – the class II object which features in Figs 7 and 8 – was also disregarded, along with the class II objects 2 and 10. Each class III object had its spectrum compared with others of a similar spectral type from each index, as in Figs 5–8. The spectra of objects 1, 3, 6, 7, 15, 16 and 22 were found to exhibit excess emission and veiling. Each spectrum was also compared, in the same manner, to every other member of the 2σ sample, irrespective of their difference in spectral types. Apart from the expected variety among objects of different spectral type, no other pattern of diversity or anomaly, other than that already discussed, was discerned.

The spectra of the remaining class III objects (Table 3) are those that, by comparison, show no evidence of excess emission, veiling or reddening. We present them as a catalogue of spectra of young brown dwarfs which, to the greatest extent discernible, are clear of contributions from sources other than their photospheres. The spectral types of the chosen objects, as determined from our near-infrared spectra, range from M5.5 to L1.1. Table 3 also includes a rough estimate of the effective temperature ($T_{\rm eff}$) of each object. The $T_{\rm eff}$ of each object was estimated using the SpT–$T_{\rm eff}$ relationship given in MuzŽić et al. (2014) for objects of spectral types later than M1. The different spectral types of each object, derived via the three different spectral indices, yielded a range of values of $T_{\rm eff}$ for each object. The $T_{\rm eff}$ listed in Table 3 is the median of these values, rounded to the nearest 50 K. The typical uncertainty in each estimated $T_{\rm eff}$ is 150–200 K. The catalogue of these spectra can be accessed at http://browndwarfs.org/sonyc.

7 CONCLUSIONS

We have carried out a near-infrared spectroscopic analysis of 30 objects in the UpSco star-forming region, 24 of which had been

Table 3. UKIDSS *Z* photometry, HPI spectral type, H_2O spectral type, H_2O–K2 spectral type and T_{eff} of the 11 objects selected as near-infrared spectral templates for young low-mass stars and brown dwarfs between M5 and L1.

Object number	2MASS name	*Z* mag	HPI spectral type	H_2O spectral type	H_2O–K2 spectral type	T_{eff} (K)
18	2MASSJ15591513-2840411	14.14	M6.8	M5.5	M5.7	3050
17	2MASSJ15582376-2721435	14.35	M6.9	M5.7	M5.6	3050
14	2MASSJ15544486-2843078	15.51	M7.1	M5.9	M6.1	3000
19	2MASSJ16002535-2644060	14.38	M7.2	M5.9	M6.2	3000
13	2MASSJ15524857-2621453	14.62	M7.1	M6.1	M6.0	3000
20	2MASSJ16005265-2812087	15.04	M7.2	M6.1	M6.8	2950
21	2MASSJ16062870-2856580	14.90	M7.5	M6.2	M5.2	3050
9	2MASSJ15493660-2815141	14.66	M7.3	M6.3	M6.0	2950
8	2MASSJ15492909-2815384	14.29	M7.3	M6.4	M6.5	2950
23	2MASSJ16101316-2856308	15.67	M7.8	M7.7	M8.0	2750
24	2MASSJ16195827-2832276	18.74	L0.3	L1.1	L0.8	2300

previously identified as brown dwarf candidates based on their photometry and proper motion alone. The resulting spectra confirm that all 24 are young very low mass objects with spectral types that range from M5.5 to L1.1.

We have observed a diversity in form among the spectra that can impact on spectral type determination. Class II objects display excess emission and veiling in their spectra. The same form of excess emission and veiling is also present in the spectra of 7 out of 18 (∼40 per cent) class III objects. This is evidence that these class III objects are still accreting from an inner disc of dust and gas which is too faint to be detected via mid-infrared photometry.

We present a catalogue of near-infrared spectra for young brown dwarfs that are clear from discernible contributions from anything other than their photospheres. We recommend the use of these objects as spectroscopic templates for identifying young brown dwarfs, and make them available at http://browndwarfs.org/sonyc.

ACKNOWLEDGEMENTS

This work was supported by Science Foundation Ireland within the Research Frontiers Programme under grant no. 10/RFP/AST2780. This publication makes use of data products from the *Wide-field Infrared Survey Explorer*, which is a joint project of the University of California, Los Angeles, and the Jet Propulsion Laboratory/California Institute of Technology, funded by the National Aeronautics and Space Administration. This publication also makes use of data products from the Two Micron All Sky Survey, which is a joint project of the University of Massachusetts and the Infrared Processing and Analysis Center/California Institute of Technology, funded by the National Aeronautics and Space Administration and the National Science Foundation. DP would like to acknowledge that her contribution was partially supported by a grant from the American Astronomical Society. We would also like to thank the UKIDSS Team for the excellent data base they have made available to the community.

REFERENCES

Allers K. N., Jaffe D. T., Luhman K. L., 2007, ApJ, 657, 511
Ardila D., Martin E., Basri G., 2000, AJ, 120, 479
Chabrier G., Baraffe I., 2000, ARA&A, 38, 337
Cushing M. C., Vacca W. D., Rayner J. T., 2004, PASP, 116, 362
Cushing M. C., Rayner J. T., Vacca W. D., 2005, ApJ, 623, 1115
Dawson P., Scholz A., Ray T. P., 2011, MNRAS, 418, 1231
Dawson P., Scholz A., Ray T. P., Marsh K. A., Wood K., Natta A., Padgett D., Ressler M. E., 2013, MNRAS, 429, 903
de Bruijne J. H. J., Hoogerwerf R., Brown A. G. A., Aguilar L. A., de Zeeuw P. T., 1997, in Perryman M. A. C., Bernacca P. L., Battrick B., eds, ESA SP-402: Hipparcos - Venice '97 Improved Methods for Identifying Moving Groups. ESA, Noordwijk, p. 575
de Zeeuw P. T., Hoogerwerf R., de Bruijne J. H. J., Brown A. G. A., Blaauw A., 1999, AJ, 117, 354
Folha D. F. M., Emerson J. P., 1999, A&A, 352, 517
Hartigan P., Kenyon S. J., Hartmann L., Strom S. E., Edwards S., Welty A. D., Stauffer J., 1991, ApJ, 382, 617
Kirkpatrick J. D., Barman T. S., Burgasser A. J., 2006, ApJ, 639, 1120
Lodieu N., 2013, MNRAS, 431, 3222
Lodieu N., Hambly N. C., Jameson R. F., 2006, MNRAS, 373, 95
Lodieu N., Hambly N. C., Jameson R. F., Hodgkin S. T., Carraro G., Kendall T. R., 2007, MNRAS, 374, 372
Lodieu N., Hambly N. C., Jameson R. F., Hodgkin S. T., 2008, MNRAS, 383, 1385
Lodieu N., Dobbie P. D., Hambly N. C., 2011, A&A, 527, A24
Looper D. L., Burgasser A. J., Kirkpatrick J. D., Swift B. J., 2007, ApJ, 669, L97
Mamajek E. E., Pecaut M. J., Nguyen D. C., Bubar E., 2013, Protostars and Planets VI, Rewriting the Star-Formation History of the Nearest OB Association. Poster #1K086
Mathis J. S., 1990, ARA&A, 28, 37
Muench A. A., Lada C. J., Luhman K. L., Muzerolle J., Young E., 2007, AJ, 134, 411
MuzŽić K., Scholz A., Geers V., Jayawardhana R., Tamura M., 2012, ApJ, 744, 134
MuzŽić K., Scholz A., Geers V., Jayawardhana R., López Martí B., 2014, ApJ, 785, 159
Pecaut M. J., Mamajek E. E., Bubar E. J., 2012, ApJ, 746, 154
Peterson D. E. et al., 2008, ApJ, 685, 313
Preibisch T., Brown A. G. A., Bridges T., Guenther E., Zinnecker H., 2002, AJ, 124, 404
Rayner J. T., Toomey D. W., Onaka P. M., Denault A. J., Stahlberger W. E., Vacca W. D., Cushing M. C., Wang S., 2003, PASP, 115, 362
Rayner J. T., Cushing M. C., Vacca W. D., 2009, ApJS, 185, 289
Rieke G. H., Lebofsky M. J., 1985, AJ, 288, 618
Rojas-Ayala B., Covey K. R., Muirhead P. S., Lloyd J. P., 2012, ApJ, 748, 93
Scholz A., Geers V., Jayawardhana R., Fissel L., Lee E., Lafreniere D., Tamura M., 2009, ApJ, 702, 805
Scholz A., Muzic K., Geers V., Bonavita M., Jayawardhana R., Tamura M., 2012, ApJ, 744, 6
Slesnick C. L., Carpenter J. M., Hillenbrand L. A., 2006, AJ, 131, 3016
Slesnick C. L., Hillenbrand L. A., Carpenter J. M., 2008, ApJ, 688, 377
Vacca W. D., Cushing M. C., Rayner J. T., 2004, PASP, 115, 389

Whitworth A., Bate M. R., Nordlund A., Reipurth B., Zinnecker H., 2007, in Reipurth B., Jewitt D., Keil K., eds, Protostars and Planets V. Univ. Arizona Press, Tucson, AZ, p. 459

SUPPORTING INFORMATION

Additional Supporting Information may be found in the online version of this article:

(http://mnras.oxfordjournals.org/lookup/suppl/doi:10.1093/mnras/stu973/-/DC1).

Please note: Oxford University Press are not responsible for the content or functionality of any supporting materials supplied by the authors. Any queries (other than missing material) should be directed to the corresponding author for the article.

This paper has been typeset from a TEX/LATEX file prepared by the author.